# フィン付き流路内の流動・熱伝達特性に関する研究

Ph.D. Dissertation

# Study on Heat Transfer and Fluid Flow Characteristics of Rectangular Finned Surface in Duct

September 2007

University of the Ryukyus
Graduate School of Engineering and Science
Material, Structural and Energy Engineering
Islam Md. DIDARUL

# Contents

# Abstract

## Study on Heat Transfer and Fluid Flow Characteristics of Rectangular Finned Surface in Duct

A detailed experimental investigation of the heat transfer and fluid flow characteristics of rectangular finned surfaces of four different fin patterns, co-angular, zigzag, co-rotating and co-counter rotating was conducted for an airflow ($Re$ = 15700 – 104500) in a duct. Short rectangular fins of either aluminum or resin material were attached in 7 × 7 arrays to a heating surface (base plate) of constant heat flux by double sided thin tape. T-type thermocouples and an infrared camera (TVS 8000) with a 160 × 120 point In-Sb sensor were used to capture the infrared images as well as to measure the temperature and the detailed heat transfer at the endwall along with fin base. Different flow visualization technique, fluorescence dye flow in water channel, smoke flow visualization and oil titanium oxide film flow visualization were used to analysis the flow behavior and its effect on heat transfer. In this study we have first investigated the heat transfer and fluid flow characteristics of co-angular and zigzag fin pattern at a flat plate (200 mm duct height) boundary layer and narrow duct of 20 mm height. Zigzag pattern were found to be more effective in heat transfer at both flat plate and narrow duct case. In case of co-angular pattern dye flow stagnated in front of the fin and formed a strong horseshoe vortex around the fin while the longitudinal vortexes generated by the side top edges touched the fin surface and the endwall. On the other hand in case of zigzag pattern a weak horseshoe vortex appeared and longitudinal vortex struck the endwall mainly and a sinusoidal wavy flow behavior was observed. We have then further investigated heat transfer and flow characteristics of co-rotating pattern and

co-counter rotating pattern along with other two pattern at a duct of 50 mm height. The heat transfer result shows that the co-rotating pattern has the highest Nusselt number and the co-angular pattern has the least Nusselt number. Considering the thermal performance, co-rotating pattern with smaller pitch ratio was found to be the most recommended pattern as the heat transfer augmentation with co-rotating pattern is more than three times the fin-less duct. Horseshoe vortex, main longitudinal vortex and rolled up vortex were again confirmed by smoke flow and oil titanium flow visualization. Among the four patterns largest friction factor occurred for the co-rotating pattern at smaller pitch ratio owing to the strong flow interactions and combined vortex attack on the endwall and fin surface whereas the least friction developed for co-angular pattern. Finally the effects of duct height on heat transfer and flow characteristics were investigated and the most important information about vortex structures at several streamwise positions was obtained which shows the reasons of heat transfer enhancement. Vortex structures for co-angular and co-rotating pattern were found different and the reattachment positions were obtained. Comparatively large scale vortex rotation was observed in co-rotating case which is obviously responsible for heat transfer enhancement.

*Keywords:* Convective heat transfer; Heat transfer enhancement; Rectangular fin; Longitudinal vortex; Horseshoe vortex; Infrared Image

# Nomenclature

$D_H$ : Hydraulic diameter of the duct, m

$D_E$ : Equivalent diameter of the duct, m

$f$ : Friction factor

$L$ : Fin length = 20 mm

$H_d$ : Height of duct 20~ 200 mm

$H_f$ : Height of fin = 5 ~15 mm

$\bar{h}$ : Average heat transfer coefficient, W/m$^2$ .K

$h$ : Heat transfer coefficient, W/m$^2$ .K

$h_x$ : Streamwise local heat transfer coefficient, W/m$^2$ .K

$h_z$ : Spanwise local heat transfer coefficient, W/m$^2$ .K

$\overline{Nu}$ : Area-averaged Nusselt number ($\bar{h}D_H / \lambda$)

$\overline{Nu}_E$ : Area-averaged Nusselt number ($\bar{h}D_E / \lambda$)

$\overline{Nu}_L$ : Area-averaged Nusselt number ($\bar{h}L / \lambda$)

$\overline{Nu}_{overall}$ : Area-averaged Nusselt number on overall surface area ($\bar{h}_{overall}D_H / \lambda$)

$\overline{Nu}_{fin}$ : Area-averaged Nusselt number on fin base ($\bar{h}_{fin}D_H / \lambda$)

$P$, $P_\infty$ : Streamwise and atmospheric pressure respectively, N/m$^2$

$t_w$ : Wall temperature, °C

$t_\infty$ : Mainstream temperature, °C

$Re$ : Reynolds number [$UD_H$/ ν]

$Re_E$ : Reynolds number [$UD_E$/ ν]

$Re_L$ : Reynolds number [$UL/\nu$]

$U$ : Mean air velocity, m/s

$PR$ : Ptch ratio

$S_x$ : Fin spacing in streamwise direction (shown in Fig. 2.1)

$S_z$ : Fin spacing in spanwise direction (shown in Fig. 2.1)

$X$ : Streamwise coordinate ($X = 0$ at the center of rectangular fin of first row)

$Z$ : Spanwise coordinate ($Z = 0$ at the center of rectangular fin of first row).

$X^*$ : Streamwise coordinate ($X^* = 0$ at the center of rectangular fin of third row)

$Z^*$ : Spanwise coordinate ($Z^* = 0$ at the center of rectangular fin of third row)

*Greek symbols*

$\alpha$ : Inclination angle

$\nu$ : Kinematic viscosity of air, $m^2/s$

$\lambda$ : Thermal conductivity, W/(m.K)

**Subsripts**

s : Smooth surface

# Introduction

## 1.1 Why heat transfer is so important?

Heat transfer or Thermal management is an important factor in engineering which have great contribution to the technological advancement of the modern civilization. Thermal management or temperature control is a great concern to heat generating bodies, as for example, power plants, nuclear reactors, engines, motors, heat exchangers, process industries, generators, electronic equipment, digital computers even though in space craft. If the heat generated in a machine is not removed at a sufficient rate, some problems, even the breakdown can take place in the machine due to overheating. This sort of problem can only be overcome by a more effective heat transfer. So a great deal of research work is going on in this field to develop a more effective technology.

## 1.2. Different methods of enhancing heat transfer

There are many ways of enhancing heat transfer. Cooling by jet spray, especially at high temperatures, vortex generators and fins or extended surfaces are very important technology and commonly encountered in heat transfer augmentation. I would like to limit my literature review on vortex generators and extended surfaces.

### 1.2.1. Vortex generators- an emerging technology

A vortex generator is an emerging technology to enhance heat transfer. Studies concerning the influence of longitudinal vortices on heat transfer are a great topic to the present

day development of high performance thermal systems. The use of longitudinal vortices generated by different kind of vortex generators to enhance the heat transfer in the air side of heat exchangers has been considered promising. Until last decade, few research works have shown the potential use of vortex generators in enhancing heat transfer in compact heat exchangers. Mostly earlier works dealt with longitudinal vortices and heat transfer related to turbine blade cooling. One of the earliest is reported by Edwards and Alker [1974], who investigated the effect of both counter rotating and co-rotating vortices on heat transfer of boundary layers. Spatially resolved heat transfer rates were determined by passing flow over a wall of uniform heat flux. Cubes and vortex generators blades were used to create the longitudinal vortices and found that the cubes produced the highest local heat transfer improvement of up to 160% while the generators effect was extended at farther downstream. The counter rotating vortex pairs showed more effectiveness than the co-rotating pairs with an increase in heat transfer of maximum 65% than flat plate values for the counter rotating vortex generators with 15° attack angle. Turk and Junkhan [1986] measured the spanwise heat transfer downstream of a rectangular blade type vortex generators mounted on a flat plate and the spanwise local heat transfer coefficients were found varying with the spanwise blade spacing. Fiebig and coworkers (1986, 1991) have conducted a series of experimental and numerical simulation about the influence of wing type vortex generators on heat transfer and pressure loss in duct flows. They tried to improve the performance of plate-fin heat exchangers. Heat transfer in fin-tube configuration was first studied by Russel et al [1982] and focused on the use of vortex generators to enhance heat transfer in fin tube configurations. Their experimental work was very promising because they showed that the vortex generators could enhance heat transfer. In a more application based experiment, Fiebig et al.[1993,1994] studied the influence of winglet type vortex generators in fin tube configurations with three tube rows and measure the heat transfer and pressure loss for different fin spacing, tube arrangement (inline or staggered) and tube form.

They found that the heat transfer coefficient was enhanced by 55% – 65% for circular tube with an inline arrangement whereas staggered arrangement caused 9%.

### 1.2.2. Extended surfaces

Fins are widely used as the primary means of heat exchanging devices. The need for more efficient cooling techniques of devices has recently prompted study into heat transfer and flow characteristics of various configurations of finned surfaces. The pin fin is a typical configuration that is often used to cool the trailing edge region of turbine blades; the internal passage of turbine blades can be very narrow, so that the choice of cooling scheme is limited. The effective heat transfer of staggered arrays of short pin fins was studied by Vanfossen [1982] and found to be half that for longer pin fins. However, this study did not detail the local characteristics of pin fin arrays. Sparrow et al. [1976] investigated the local heat transfer coefficient over a plate surface by the naphthalene sublimation technique for a two-row plate fin and tube heat exchanger, finding that the coefficient was lowest behind the pin. The effect of pin fin arrangement on heat transfer over an endwall, the heating surface where the fins are attached, was examined using a thermo sensitive liquid crystal film by Matsumoto et al. [1997], who concluded that the heat transfer from the endwall was enhanced by flow acceleration between the pin fins rather than the horseshoe vortex around the pin. Rectangular fin is found to have an extensive use in heat exchanger surfaces and in many applications. Geometric parameters, such as aspect ratio, fin height to duct blockage ratio, fin inclination angle, orientation of fin i.e. fin pattern, fin pitch ratio in stream wise and span wise direction and fin shapes have pronounced effects on the local and overall heat transfer coefficients as well as on the thermal performance of the heat exchanging devices. With the increasing demand of compact, light weight high performance heat exchanging devices researchers are trying hard to serve the fins as extended

surface as well as vortex generator to obtain the combined effect of extended surface and vortex generator which is an emerging technology in the field of heat transfer.

Recently, inclined rectangular fin embedded to the endwall is found to be an effective configuration for heat transfer enhancement, because the inclined fin produce the longitudinal vortex of which intensity exist at far downstream. It is expected that the heat transfer from the endwall and the fin surface can be improved by this inclined fins and hence this configuration is identified as being very promising. Torii and Yanagihara [1997] has reviewed on heat transfer enhancement by longitudinal vortices and discussed how longitudinal vortices are produced by different kind of vortex generators and enhances heat transfer. That review focused on the effect of longitudinal vortices generated by wings on the heat transfer enhancement in boundary layers, ducts and plate fin tube geometries. Heat transfer enhancement in arrays of rectangular blocks has been investigated by many researchers. Sparrow et al. [1982, 1983] studied the heat transfer and pressure drop characteristics of arrays of rectangular modules commonly encountered in electronic equipment. In their experiment, heat transfer enhancements exceeding a factor of two were achieved by the use of multiple fences like barriers, with the inter barrier spacing and the barrier height being varied parametrically along with the Reynolds number. Igarashi [1983] studied heat transfer from a square prism with different inclination angles and observed reattachment flow for inclination angles of 14°–35°. Heat transfer from an array of parallel longitudinal fins to a turbulent air stream passing through the inter fin spaces has been investigated both numerically and experimentally by Kadle and Sparrow [1986]. They found that the local heat transfer coefficients varied both along the fins and the surface of the base plate. Oyakawa et al. [1993] studied the heat transfer of plate setting rectangular fins with inclination angle of 20° and showed that this configuration can enhance heat transfer. Molki et al. [1995] experimentally studied the heat transfer at the entrance region of an array of rectangular heated blocks and presented empirical correlations of the heat transfer for the array. El-Saed et al.

[2002] investigated heat transfer and fluid flow in rectangular fin arrays and found that the mean Nusselt number increases with increasing Reynolds number, inter-fin space and fin thickness but did not examine endwall heat transfer. Bilen and Yapici [2002] investigated heat transfer enhancement from a surface fitted with rectangular blocks at different inclination angle and found that the maximum heat transfer was obtained at an angle of 45° while the effect of inclination angle is little for larger than 22.5°, though the local heat transfer characteristics were not reported.

In contrast to rectangular fins, cylinder-like pin fins have been found to exhibit a large pressure drop due to the drag force and flow acceleration or deceleration through the fins. This difference is due to the fact that rectangular arrays do not form extremely narrow passages, which also causes the heat transfer for rectangular fins to be relatively lower. However, the poor heat transfer region behind the pin may be improved by longitudinal vortexes generated by the fin. Furthermore, when the fin array is set such that the inclination angle of every row is changed alternately, the longitudinal vortex produced by the top edge of the fin reattaches to that of the following fin increasing the heat transfer from the fin surface. As the above literature review shows, previous studies have investigated heat transfer enhancement from surfaces with arrays of short rectangular fins and a few studies have concentrated on heat transfer from endwall for short rectangular fins with different inclination angles. However, a detailed heat transfer analysis from an endwall with arrays of short rectangular fins of different patterns (co-angular, zigzag, co-rotating and co-counter rotating) in the duct flow has not yet been completed. Bilen and Yapici [2002] have conducted a study for the co-angular case only, but did not clarify the local heat transfer characteristics. In co-angular pattern, fins arranged at same angle to the same direction at each and every row. This inclination angle of the fins will form longitudinal vortex which will strike the next fin surface and endwall. Flow will touch both sides of the fin surface and so it is expected the extended surface effect will be higher than vortex effect on the endwall. When the

fins are set at same angle at each row but the directions are alternately changed then we define that pattern as zigzag pattern. Due to the alternate directions of the fins, a sinusoidal wavy flow behavior is expected to observe which will increase the vortex effect on the endwall more than the extended surface effect. In co-rotating and co-counter rotating pattern, fins are set in such a way that it forms converging and diverging fin pairs in a row. In co-rotating pattern the converging and diverging fin pairs remain same at corresponding fin rows. In co-counter rotating pattern the converging and diverging fin pairs are alternately changed. This diverging fin pairs will form a couple of longitudinal vortex which might strikes the endwall strongly and this combined down wash is expected to enhance heat transfer from the endwall significantly.

### 1.3 Objective of this research.

Therefore, we have investigated the heat transfer enhancement for fin arrays of four different patterns at narrow and tall duct by setting short rectangular fins on a duct wall. We have chosen the four fin patterns, because the orientations of the fin pattern greatly affect the flow field and as a result heat transfer is augmented. In this study, short rectangular fins with four different patterns, are investigated because of its significant heat transfer enhancement caused by the large scale vortex effect and extended surface effect. In addition to, determining the overall heat transfer of the rectangular fin array, the relative magnitudes of heat transfer between the fins and endwall can be determined in this study. This study attempts to analyze the detailed heat transfer characteristics of fin base and endwall surface for different fin patterns and examine the extended surface effect from the fin surfaces and the vortex effect on the endwall for varying pitch ratio in streamwise direction. Detailed heat transfers, as well as average heat transfer coefficients are estimated from the infrared images of the representative fin region. The flow behavior around the fins is further analyzed to determine the relation between the heat transfer and fluid flow characteristics. Furthermore we discussed the thermal performance of the four

different fin patterns under the constant pumping power condition, because the heat transfer enhancement always accompanies the drag force and pressure drop simultaneously. So we might compare the heat transfer enhancement rate of this system with that of smooth duct.

# 2

# Experimental Apparatus and Procedure

## 2.1 Introduction

In this section we have mainly discussed the different fin patterns and the experimental setup for the heat transfer measurements, pressure drop measurements and flow visualization technique. Heat transfer coefficients were measured by two types of apparatus; heat transfer measurement by T types thermocouples soldered on the back side of the heating surface and the other type is heat transfer measurement by infrared camera.

## 2.2 Fin patterns and arrangements

Four types of fin patterns are studied in this research work as shown in Fig.2.1 The fins were made of either aluminum or resin materials and were rectangular with dimensions 20 mm long, 5 mm thick and three heights, 5, 10 and 15 mm. The fins were set in lines and rows of seven each. Fin spacing, fin center to center distance $S_x$, in streamwise direction were maintained 40 mm, 60 mm and 70 mm whereas $S_z$ in spanwise direction was 40 mm. The ratios $S_x/L$ and $S_z/L$ are defined as pitch ratio, $PR$ hereafter. The angles of the fins to the flow direction were maintained at $\alpha$ = 0°, 20° and 25°. In the co-angular pattern the fins were set at the same angle and in the same direction. In the zigzag pattern the fins have the same angle but are set in alternate directions after each row. In case of co-rotating pattern fin pairs are rotated in same direction and form convergent and it becomes same at every fin rows. Contrarily, in case of co-counter rotating pattern fin pairs are set as convergent and divergent alternately at row-wise direction.

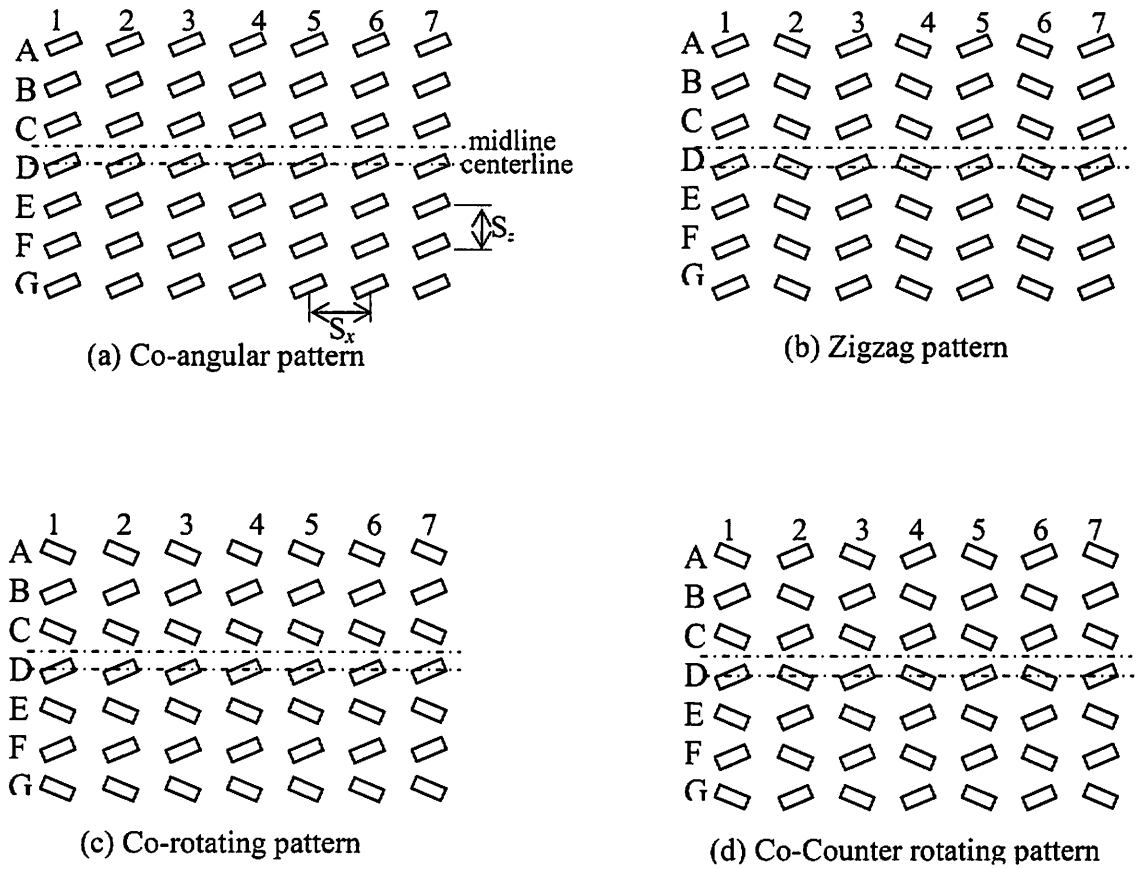


(a) Co-angular pattern

(b) Zigzag pattern

(c) Co-rotating pattern

(d) Co-Counter rotating pattern

**Fig. 2.1** Different types of fin patterns

## 2.3 Experimental setup for heat transfer measurement

### 2.3.1 Fins inside the duct

Experiments were conducted in long rectangular ducts both of 20 and 200 mm height, 230 mm span width and 784 mm length. The first row of fins was located 200 mm away from the duct entrance. The experimental apparatus and fin settings are shown in Fig.2.1. As shown in Fig. 2.2 for a duct height of $H_d$ = 200 mm, the velocity field does not develop over the test section, but rather it assumes fins are in flat plate boundary layer. On the other hand, at $H_d$ = 20 mm the flow is fully developed. The fins were attached to the lower wall of the duct by means of a 100 μm double sided thin tape. The upper plate of duct was made of a transparent acrylic resin plate for observation of the interior of the duct.

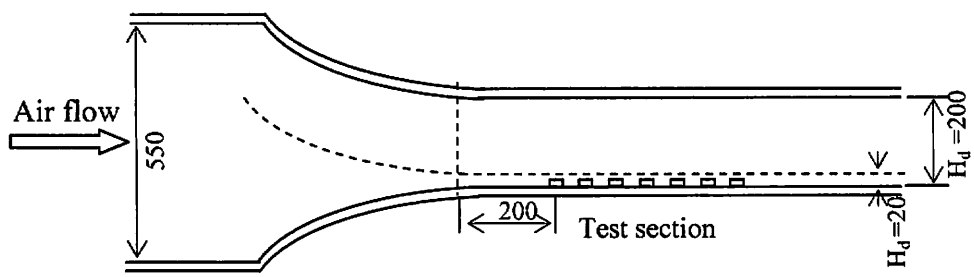


Fig.2.2 Fins inside the duct (all dimensions are in mm)

### 2.3.2 Heating surface with fins

To measure the local heat transfer coefficients, the lower wall was formed of a Bakelite plate of thickness 10 mm and a 30 μm thick stainless steel foil (200 mm × 784 mm) as a heating surface. A constant heat flux $q''$ was formed at the heating surface using a direct current source. To prevent heat loss from the heating surface through the lower wall, a layer of glass wool was placed under the Bakelite plate. The wall temperature $t_{wx}$ was measured using 70 μm diameter T-type thermocouples, soldered on the back side of the lower wall at 58 discrete locations along the centerline of the heating surface and the midline between the fins in the spanwise direction, as shown in Fig.2.3.

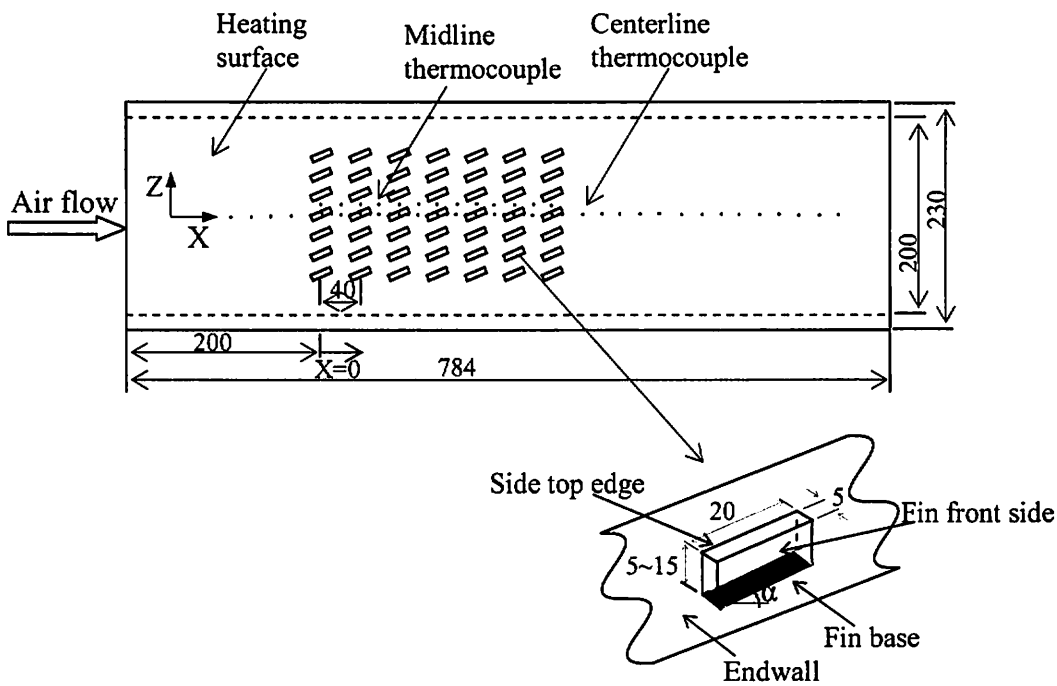


Fig.2.3 Heating surface with thermocouple locations (Dimensions in mm)

### 2.3.3 Infrared image technique

In order to observe the distributions of the temperature and the heat transfer coefficients around the fins at the endwall, infrared images were taken using an infrared camera with a indium-antimony (In-Sb) sensor, which can measure the temperature at 160 × 120 points with a resolution of 0.025°C for a black body. Here it should be mentioned that another heating surface similar to the previous one is made except the thermocouples attachments. In this case, the temperature was measured at the back of the heating surface through a window covered by polyvinyledene film with a transmissivity for infrared energy of nearly unity. The back of the heating surface was painted black and the whole experimental apparatus was covered by black cloth to ensure that the surroundings were completely dark as shown in Fig.2.4.

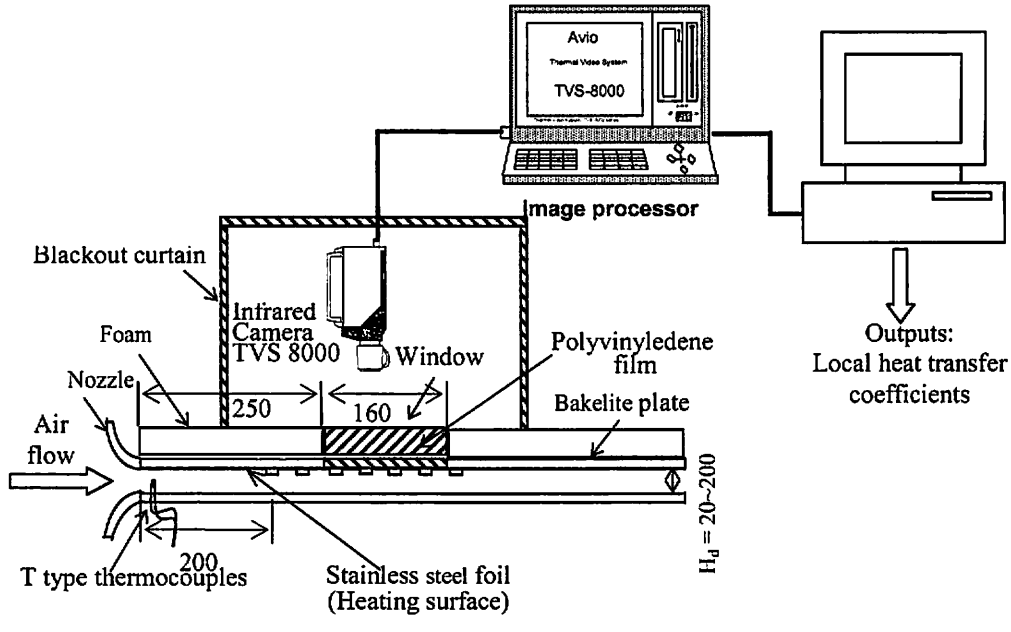


Fig.2.4 Infrared image technique

First, we measured the heat transfer using the thermocouples in the larger region to determine the effect of the fin setting. We then estimated the detailed heat transfer and averaged Nusselt numbers in the representative region by the infrared image technique.

### 2.3.4 Insulation Technique

Figure 2.5 (a) and (b) shows the thermal insulation of the heating surface with thermocouples and without thermocouples respectively. The stainless steel foil, attached to the bakelite plate was used as the heating surface and that bakelite plate was covered with 60 mm thick insulator, foam to prevent heat loss from the back of the heating surface. Therefore heat losses from back of the heating surface except window may assume to be very little. The measurement window was covered with two layers of polyvinyledene film with 1 mm space clearance. Heat losses were 1.3% of the heat flux supplied to the surface by measurement of temperature difference between heating surface and back surface.

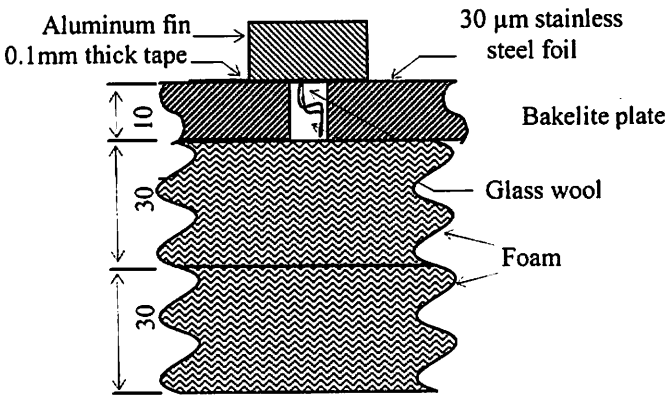


(a) Thermal insulation of the heating surface attached with thermocouples.

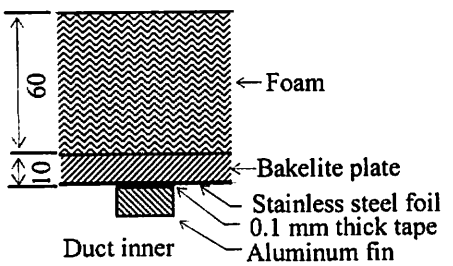


(b) Thermal insulation of the heating surface except window

Fig.2.5 Thermal insulation technique (dimensions are in mm)

## 2.4 Experimental apparatus for pressure drop measurement

To measure the pressure drop resulting from the presence of the fins, 0.5 mm diameter static pressure taps were placed at 13 various locations of upstream and downstream of the fins on the pressure plate with 60−120 mm space interval. Experimental apparatus for pressure drop measurement is shown in Fig.2.6. Here the pressure plate is a polished aluminum plate and the fins were set on the plate by double sided thin tape. Pressure was measured by a digital micro manometer with an accuracy of ± 0.1 mm $H_2O$.

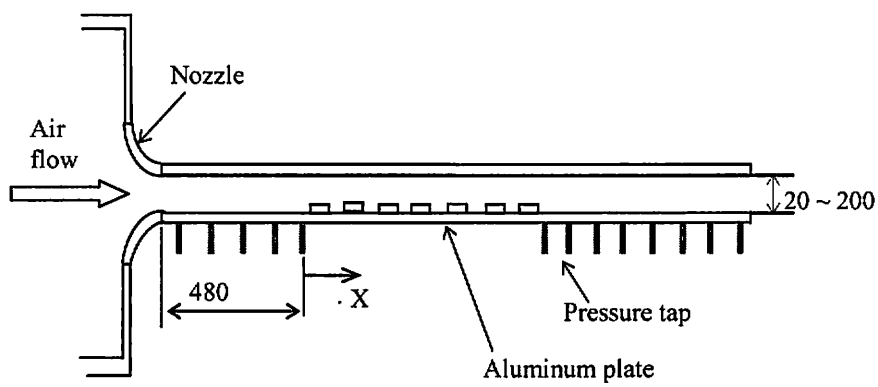


Fig. 2.6 Experimental set up for pressure drop measurement (dimension in mm)

## 2.5 Flow visualization apparatus

In order to observe the basic flow pattern and the flow behavior around the fin, flow visualization is very important. There have been used different methods to visualize the flow behavior. In our experiment, the fluid flow was visualized as follows: Dye flow in water channel, Titanium oxide oil film flow visualization and smoke flow visualization.

### 2.5.1 Experimental setup for die flow in water channel

Dye flow in water channel is one of the good visualization techniques to get a clear view of the flow pattern. Figure 2.7 shows the experimental setup for dye flow in water channel. Flow was visualized by inducing fluorescent dye in the water channel at lower Reynolds number to observe the flow pattern clearly. The water channel was made of a transparent acrylic plate of

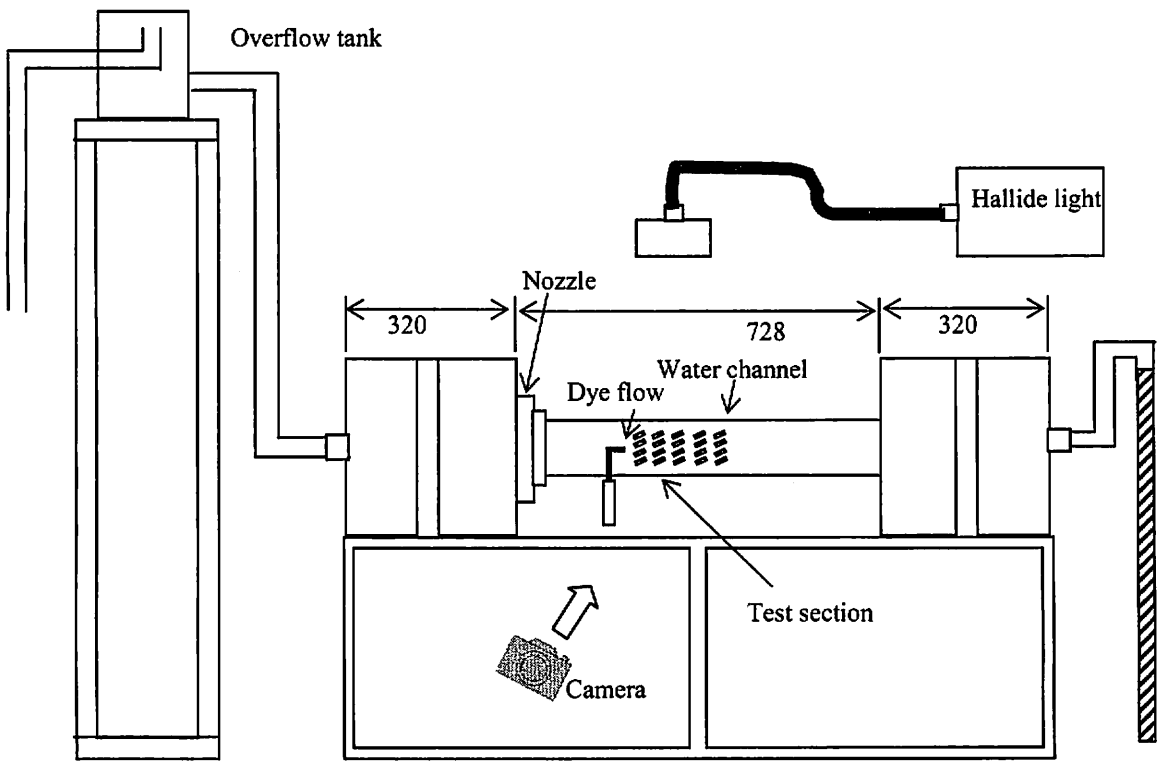


Fig.2.7 Experimental apparatus for dye flow in water channel

dimension 50 mm height and 200 mm width. Fins were attached to the side wall as shown in Fig.2.7. Fluorescent dye was induced just at the front of the fins by a narrow tube. A metal halide light set at the top of the channel and a digital camera (Nikon D70) set perpendicular to channel side wall were used to observe and shot the photographs at proper time.

### 2.5.2 Experimental setup for smoke flow visualization

In order to determine the flow behavior in details around the rectangular fin of different pattern, the fluid flow was visualized by flash light sheet method using smoke as a tracer supplied at upstream side at lower Reynolds number. Smoke flow visualization apparatus is shown in Fig.2.8. It consists of a rectangular duct made of transparent acrylic sheet, green Nd: YAG laser light, digital camera (Nikon D70) and a smoke generator that produce smoke of fine droplet of diameter 0.3 ~ 1 μm. For smoke flow visualization fins were made of transparent acrylic sheet. The Nd: YAG laser sheet which was used has an emitted radiation of wavelength of 532 nm. Camera was positioned at top of the duct and the laser light was set at the side of the duct parallel to the lower wall of the duct where the fin set. Once the camera and laser sheet were positioned, the smoke generator supplied the smoke at the entrance of the duct, then images of flow pattern were recorded.

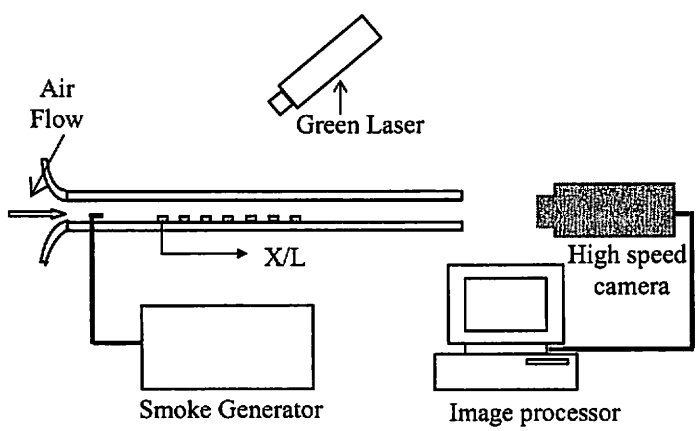


Fig.2.8 Experimental apparatus for smoke flow visualization

### 2.5.3 Experimental setup for oil titanium oxide film flow visualization

Experimental set up for the oil titanium oxide film flow is shown in Fig.2.9. Titanium oxide oil film flow patterns at the lower wall around the fins were observed at the same Reynolds number of that of the main experiment flow. In this experiment, a thin black film was attached to the lower wall and black painted fins were attached to the film. The lower wall and the fin surface were painted by a mixture of titanium oxide, linseed oil and oleic acid of suitable density and were exposed to air flow to observe the oil titanium oxide film flow. After completion of the run, photographs were taken by a digital camera (Nikon D70).

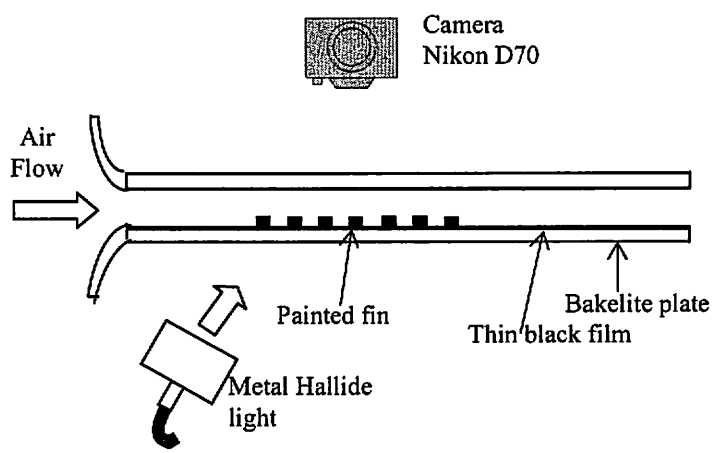


Fig.2.9 Experimental apparatus for oil titanium oxide film flow visualization

# 3

# Data Reduction and Uncertainty Analysis

## 3.1 Introduction

In this chapter data reduction, heat balance and uncertainty analysis are described, because the heat balance and uncertainty analysis are very important for the reliability of the experimental study.

## 3.2. Data reduction

In this study we have investigated the fluid flow and heat transfer. The essential quantities determined were the friction factor and the heat transfer coefficients for the different fin patterns.

The total heat generated from the heating surface is distributed into the heat transferred by convection to the flowing air, heat losses through the insulation and the window. Heat losses from back of the heating surface except window may assume to be very little as the bakelite plate was insulated by 60 mm thick insulator, foam to prevent heat loss. It was found that the heat loss from window was 1.3% of the heat flux supplied to the heating surface. So its value is so small compared to the heat input value and it can be neglected. Consequently the total heat transferred by convection to the flowing air equals the heat flux supplied to the heating surface.

The friction factor $f$ was evaluated from the pressure difference between points just upstream and downstream of the fins attached to the heating surface using the Eq.(3.1)

$$f = P_{loss} (D_H/l)/ (\rho_a U^2/2), \qquad (3.1)$$

where $l$ is the distance to the reference region, i.e. the distance between just upstream of D1 fin and downstream of D7 fin and $D_H$ is the hydraulic diameter of the duct.

The heat transfer coefficients,

$$h = \dot{q}/(t_w - t_\infty), \qquad (3.2)$$

were obtained at representative region, where $t_w$ is the wall temperature and the $t_\infty$ is the mainstream temperature.

We considered three kinds of Reynolds numbers and examined their effects on the heat transfer characteristics at the flat plate boundary layer and the narrow duct with fin arrays. Reynolds number based on the mainstream velocity and fin length can be expressed as

$$Re_L = UL/\nu \qquad (3.3)$$

Reynolds number based on the mainstream velocity and the duct hydraulic diameter and can be expressed as

$$Re = UD_H/\nu \qquad (3.4)$$

Reynolds numbers is based on the mean velocity and the duct equivalent diameter and can be expressed as

$$Re_E = UD_E/\nu \qquad (3.5)$$

The area-averaged Nusselt number based on the duct hydraulic diameter can be expressed as

$$\overline{Nu} = \bar{h}D_H/\lambda. \qquad (3.6)$$

The area-averaged Nusselt number based on the duct equivalent diameter can be expressed as

$$\overline{Nu_E} = \bar{h}D_E/\lambda. \qquad (3.7)$$

The area-averaged Nusselt number based on the fin length can be expressed as

$$\overline{Nu_L} = \bar{h}L/\lambda \qquad (3.8)$$

### 3.3 Uncertainty analysis

The pressure was measured by a digital micro manometer of accuracy ± 0.1 mm of $H_2O$. The heating surface was covered with 60 mm thick insulator, foam to prevent heat loss from the heating surface. Therefore heat losses from back of the heating surface may assume to be very little. Window was covered with two layers of polyvinyledene film with 1 mm space clearance and heat losses were 1.3% of the heat flux supplied to the surface. As a result, heat transfer coefficient contained less than 3% uncertainty. The temperature was measured by both the thermocouples using a data logger and the infrared camera. The percentage relative uncertainty in the measured temperature for the thermocouples and the infrared camera were ± 0.25% and ± 1.3% respectively. The percentage relative uncertainty in the measured electric power input was ± 1.4%. The percentage relative uncertainty in the compound variables were found to be less than ± 5% both for the velocity and the Reynolds number and ± 3% both for the heat transfer coefficient and Nusselt number.

# 4

# Heat Transfer Characteristics and Flow Analysis of Finned Surfaces in Case of Tall Duct and Narrow Duct.

## 4.1 Introduction

In this chapter we would like to discuss the heat transfer characteristics and fluid flow analysis of finned surfaces of co-angular and zigzag pattern. Experiments were conducted for fins setting at a flat plate boundary layer i.e. in tall duct and narrow duct corresponding to 200 mm and 20 mm duct height.

## 4.2 Local heat transfer coefficients

### 4.2.1 Smooth duct results

The distributions of the local heat transfer coefficients $h_x$ at the endwall without rectangular fins are shown in Fig. 4.1. To check the accuracy of the heat transfer measurements and to determine the characteristics of both ducts without fins, we measured the local heat transfer coefficient on the smooth duct surface. Fig. 4.1(a) presents the streamwise distributions of the local heat transfer coefficient along the endwall from the duct entrance in the duct of $H_d$ = 200 mm for $U$ = 5, 10 and 20 m/s. The distributions gradually decrease in the streamwise direction. Since the duct height was so large, both the hydrodynamic and thermal boundary layers were still developing, even at the test section. Due to the rough surface at the duct inlet, acting as a tripping surface, the flow was turbulent. The local Nusselt number, based on $h_x$ and the distance, $X$ from entrance agrees with the equation

$$Nu_x = 0.0296 Re_x^{0.8} Pr^{0.6} \qquad (4.1)$$

for a turbulent boundary layer on a flat plate, as shown by the solid lines in Fig.4.1 (a). In the figure, the open and solid symbols designate the centerline and the midline, respectively. Both sets of data are equal regardless of spanwise position indicating the two dimensionality of the

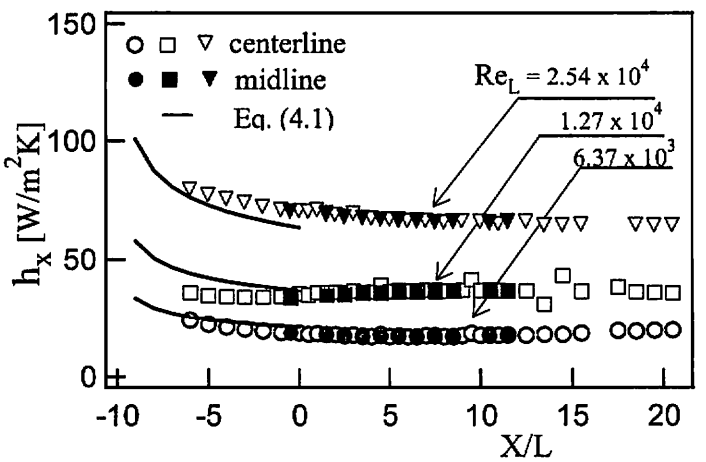


(a) $H_d$ = 200 mm

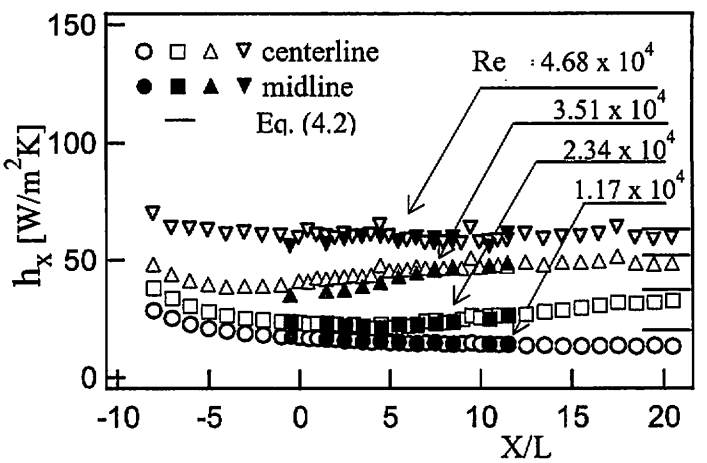


(b) $H_d$ = 20 mm

Fig. 4.1 Local heat transfer distributions without fin on smooth surface

heating surface. The data shows good agreement with Eq. (4.1).

The results for the narrow duct are shown in Fig. 4.1(b). The distributions gradually decrease toward the downstream direction at lower Reynolds numbers. At $Re$ = 2.34 × $10^4$ and

$3.51 \times 10^4$, the distribution slowly increases and coincides with the following equation for a fully developed hydrodynamic boundary layer for air flow at the downstream region as shown by the solid lines:

$$Nu = 0.019Re^{0.8} \qquad (4.2)$$

Hence the duct heights of $H_d$= 200 mm and $H_d$ = 20 mm represents a flat plate turbulent boundary layer and a fully developed duct flow in test section, respectively.

### 4.2.2 Effect of inclination angles on heat transfer

The effect of the inclination angle of the rectangular fin on the local heat transfer coefficient is presented in Figs. 4.2.(a), (b), and (c) for $\alpha$ = 0°, 20° and 25°, respectively. Each graph represents the streamwise local heat transfer coefficient at the centerline and at the midline. Centerline and midline data are calculated along the center of the fin rows and middle between fin lins respectively as shown in Fig.2.1. The data for the centerline decreases gradually up to the first row of fins, where it exhibits a rapid increase and attains a maximum value before rapidly decreasing to a minimum value, with the pattern repeated periodically. Maximum values are obtained at fin positions and the minima are obtained between the fins along the streamwise direction. The maximum value at the fin center may be the combined effect of the extended surface and longitudinal vortex. Even the minimum values are higher than those without fins and hence it may be considered that heat transfer is enhanced by turbulence or large scale vortexes generated by the fins. The solid symbols in the figure describe the heat transfer enhancements at the endwall caused by the longitudinal and other vortexes. As the longitudinal vortex formed by the top surface of the fin strikes the endwall between fins so the heat transfer is augmented of that region. At the same time turbulence caused by the corner edge also increases the flow mixing; as a result heat transfer is increased behind the fins. Fig. 4.2(a) shows the periodical

distribution for $\alpha = 0°$ while the heat transfer increases between the fins in the spanwise direction and decreases at other places. Though the heat transfer coefficients along the centerline position of the fin for $\alpha = 20°$ (Fig. 4.2(b)) and 25° (Fig. 4.2(c)) increases in the same manner as for $\alpha = 0°$, the heat transfer coefficients along the midline are somewhat different. Along the midline, the local heat transfer coefficients are affected by the longitudinal vortex, maintaining large values for $\alpha = 20°$ and 25° compared to 0°. The heat transfer coefficient for $\alpha = 20°$ is comparatively higher among the three inclination angles, which agrees with the data obtained by Bilen et al. [2002] who found that the effect of inclination angle on heat transfer enhancement is small for inclination angles for larger than 22.5°. An inclination angle of 20° caused considerable enhancement in heat transfer. This is because of the edge effect of the rectangular fin, which increases the flow mixing. When the fins are turned around the mid point, the side edges can produce more turbulence. Because of turning around mid point, the fin will act as vortex generator and produce the longitudinal vortex constructing trailing vortex, corner vortex and induced vortex. The longitudinal vortex is also called the streamwise one which axis is in same direction as the streamwise, and persists over a long streamwise distance, disturbing the entire velocity field and temperature field. As a result heat transfer rate increases. Also the corner edges increases the turbulence level. This situation has been discussed by Herman [1994] and Herman and Kang [2001]. Therefore, an inclination angle of 20° is preferred for further analysis.

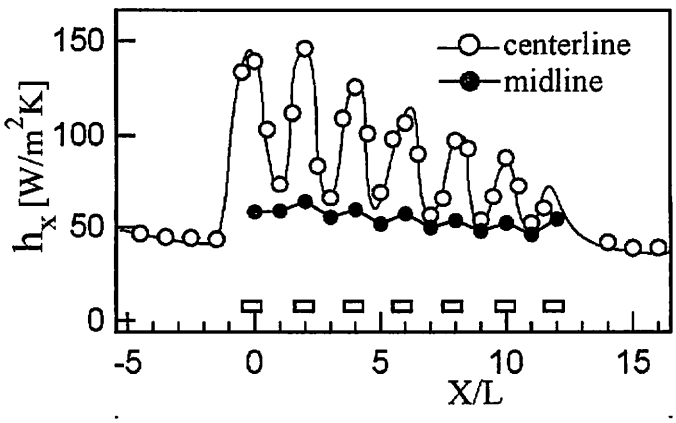


(a) $\alpha = 0^\circ$

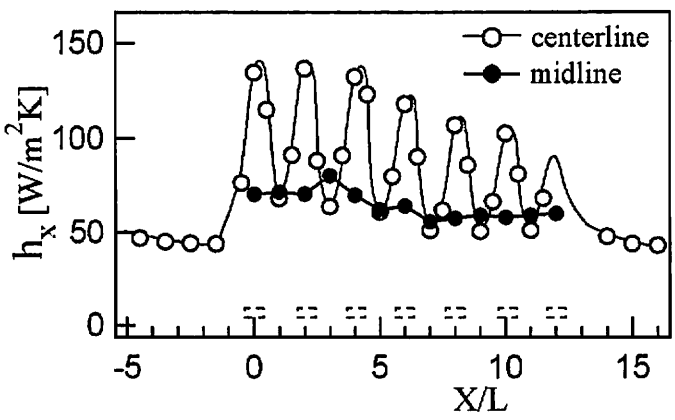


(b) $\alpha = 20^\circ$

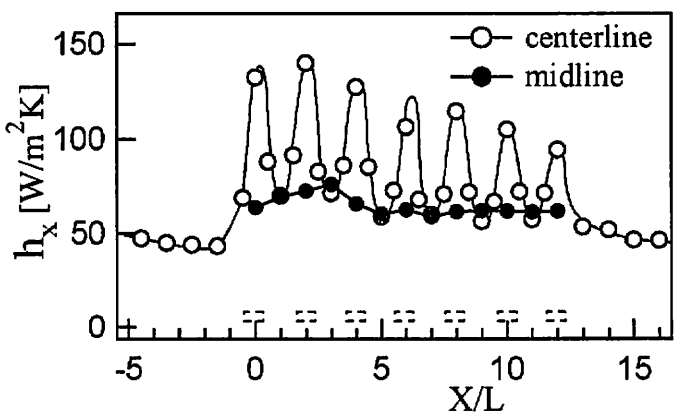


(c) $\alpha = 25^\circ$

Fig. 4.2 Effect of inclination angle on local heat transfer coefficients for $H_f = 10$ mm, $H_d = 200$ mm and $U = 10$ m/s

### 4.2.3 Heat transfer through fin of resin material

We now want to discuss the fin material with regards estimating the effect of a vortex generator on the endwall, but not for the extended surface. The local heat transfer coefficient was measured for a resin material fin, rather than an aluminum fin. The results are presented in Fig.4.3. In this figure centerline distribution shows that the heat transfer coefficient at the fin position for the resin material in contrast to the aluminum fin as shown in Fig.4.2 (b) is smaller, because of no extended surface effect. The coefficient at the midline also appears to be equal to that of the centerline. So the overall heat transfer may be enhanced by a factor of about two times than that of without fins. This results in the effect of vortex generator with no effect from

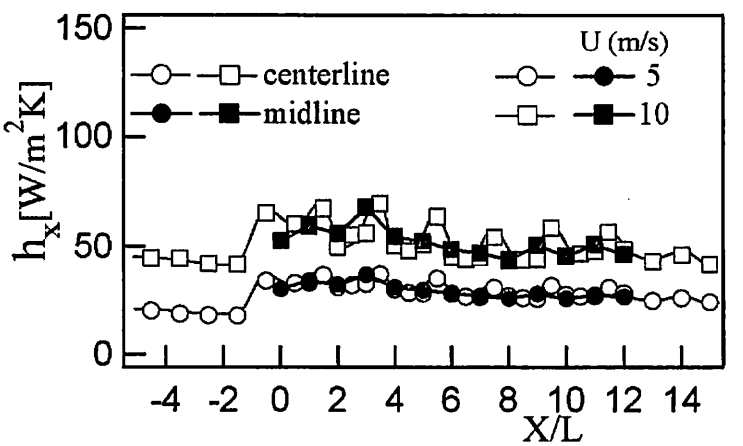


Fig.4.3 Variation of local heat transfer coefficients for resin material with $\alpha = 20^{\circ}$, $H_f = 10$ mm, $H_d = 200$ mm.

extended surface. Because the Biot number for the resin material was estimated 10 and the conduction resistance of resin material was nearly equal to the thermal resistance. Therefore, the heat transfer enhancement by an aluminum fin only will be discussed in the present experiment as the aluminum fins will have the effect of extended surface and the vortex generator at the same time. As mentioned, thin double-sided tape of thickness 100 μm was used to attach the fin to the heating surface. For the aluminum fin, the conduction resistance of the tape was 5% of the

total resistance (for an average heat transfer coefficient $\bar{h}$ assumed to be 200 W/m$^2$K). Therefore, the tape did not have much affect on the estimation of the heat transfer coefficient. Also, the Biot number, *Bi* of the aluminum fin was about 0.009, which is small enough. Therefore, the heat transfer enhancement by aluminum fin only will be discussed hereafter.

### 4.2.4 Effect of fin height on heat transfer characteristics

The effect of the height of the fin on the local heat transfer coefficient is now discussed. Fig. 4.4 shows the streamwise local heat transfer coefficient distribution for varying fin height in case of co-angular pattern at a flat plate boundary layer as a typical example. It was found that as the fin height increases, the extended surface area also increases and as a consequence the heat transfer rate increases. The local heat transfer coefficient shows a periodic distribution regardless of fin height. The difference in the heat transfer enhancement between fin heights of 10 mm and 15 mm was very small, while the difference between fins of 5 mm height and other fins was larger. Considering the larger pressure penalty for 15 mm height fin, 10 mm height fin was chosen as a typical fin.

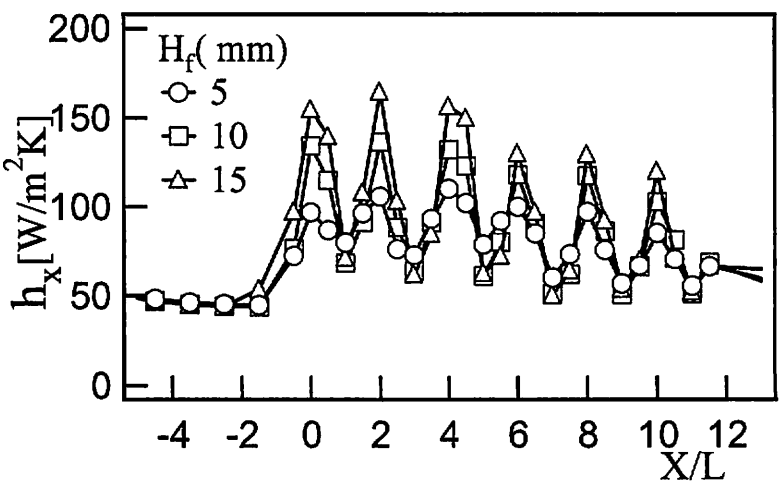


Fig.4.4 Effect of fin height on local heat transfer coefficient along centerline at co-angular pattern for $H_d$ = 200 mm and $U$=10 m/s

### 4.2.5 Effect of velocity on heat transfer characteristics

The effect of velocity on the local heat transfer coefficient in a duct of 200 mm height for a co-angular pattern is shown in Fig. 4.5(a). The local heat transfer coefficient slowly decreases in both the upstream and downstream region, while at the finned region a periodic distribution appears which is independent of velocity. The distribution for the zigzag pattern is similar to that of the co-angular pattern, as shown in Fig. 4.5 (b), though with some differences. For the zigzag pattern, the heat transfer coefficient profile near the lower peaks appears concave and shows higher values than that of the co-angular pattern. The peak values in the upstream region are higher for the co-angular pattern than for the zigzag pattern. This is because in the case of the co-angular pattern the flow touches both sides of the fins strongly and then continues smoothly whereas for the zigzag pattern the flow strongly touches the endwall and the front side of the fin while the other side remains untouched. Thus, the extended surface is more effective in the case of the co-angular pattern for a flat plate boundary layer. Fig. 4.5 (c) shows the distribution of the heat transfer coefficient for the zigzag pattern in a narrow duct. In this figure the upper peak values are found to be the highest because the upper wall of the narrow duct causes the flow to strike the endwall and the fin more strongly. Data for the co-angular pattern for the narrow duct is not shown but the distribution was almost the same as that for tall duct. In Fig. 4.5 (a) – (c), the maximum heat transfer coefficient shows some discrepancy at some streamwise velocities due to small deflections of the thermocouples from the centerline.

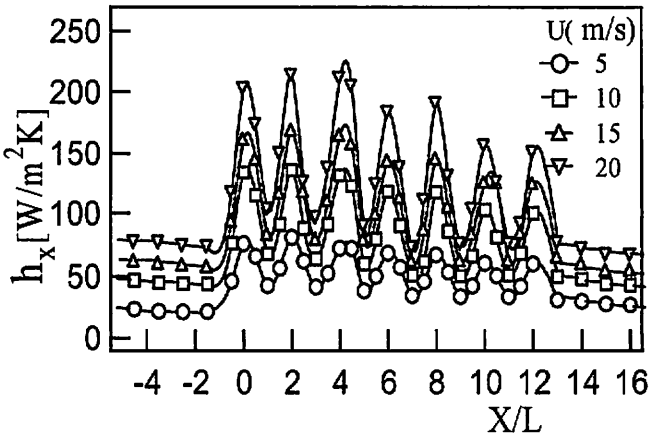


(a) Co-angular pattern, $H_d$ = 200 mm

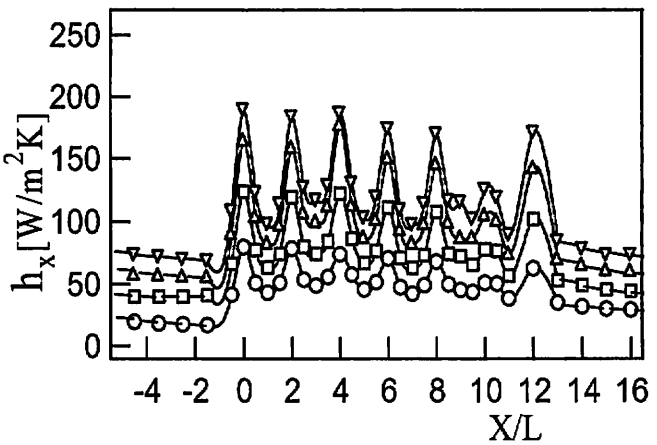


(b) Zigzag pattern, $H_d$ = 200 mm

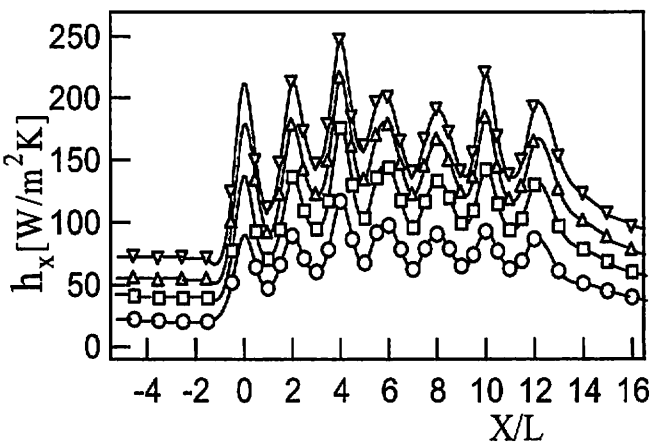


(c) Zigzag pattern, $H_d$ = 20 mm

Fig. 4.5 Variation of local heat transfer coefficient with velocity along centerline for $H_f$ = 10 mm

### 4.3 Detailed heat transfer analysis

Detailed heat transfer coefficient distributions at the endwall surfaces for rectangular fins of both co-angular and zigzag patterns for a flat plate boundary (tall duct) and narrow duct flow are shown in Figs. 4.6–4.9. As shown in Figs. 4.6(a) and 4.7(a), the heat transfer coefficient value is high around the fin rows for both patterns. These higher heat transfer regions are the combination of extended surface effect and vortex effect. At flat plate boundary layer, i.e in tall duct case, infrared image view of the co-angular pattern shows the difference of heat transfer value. At narrow duct case, co-angular pattern experiences higher heat transfer than that of tall duct case. This difference is apparently shown both at the fin base and endwall surface. Because upper wall of the narrow duct influences the flow behavior and as a result flow strikes the fin surface as well as downwash the endwall more strongly. So heat transfer coefficient value is higher at fin base and at the endwall. On the other hand upper wall of the tall duct could not have much influence on the flow behavior, so the flow did not contact the fin surface and endwall as strongly as narrow duct. As a result comparatively lower heat transfer coefficient values are observed at flat plate with co-angular pattern. Same to the co-angular pattern zigzag pattern experiences the effect of duct height on heat transfer as viewed by the infrared image with zigzag pattern. Comparing values of $h_x$ between the two patterns shows that the higher heat transfer regions increases for zigzag pattern. In the co-angular pattern, the horseshoe vortex is responsible for the enhancement of the heat transfer around the fins. The heat transfer in the region between fins in the spanwise direction is also enhanced due to lateral mixing. In the zigzag pattern, the horseshoe vortex as well as the vortex generated by the side top and corner edges strongly touches the alternately angled fin surfaces and endwall, which significantly enhances the heat transfer. Next we will discuss more detail graphical presentation of the heat transfer coefficient for the different fin pattern.

Figs. 4.6(b) and 4.7(b) show the heat transfer distribution along the centerline and midline.

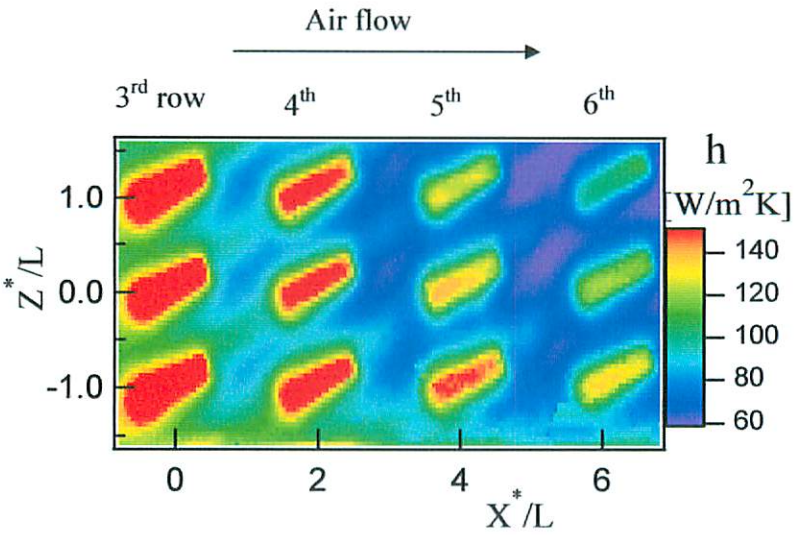


(a)

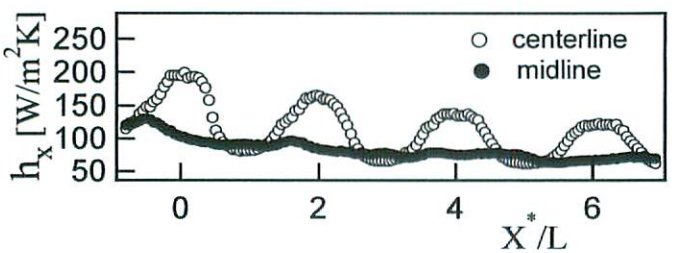


(b)

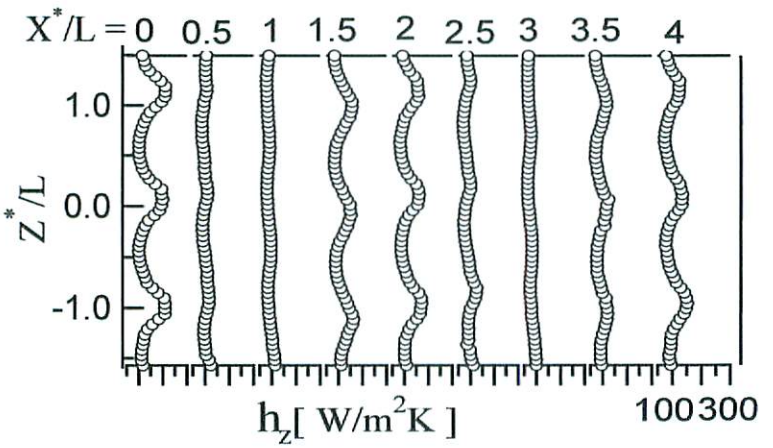


(c)

Fig. 4.6 Detailed heat transfer coefficient distributions around the representative fins of co-angular pattern at the endwall in a flat plate boundary layer for $Re_L = 1.27 \times 10^4$, $H_f = 10$ mm. (a) Infrared image. (b) Centerline and midline distributions and (c) Spanwise distributions.

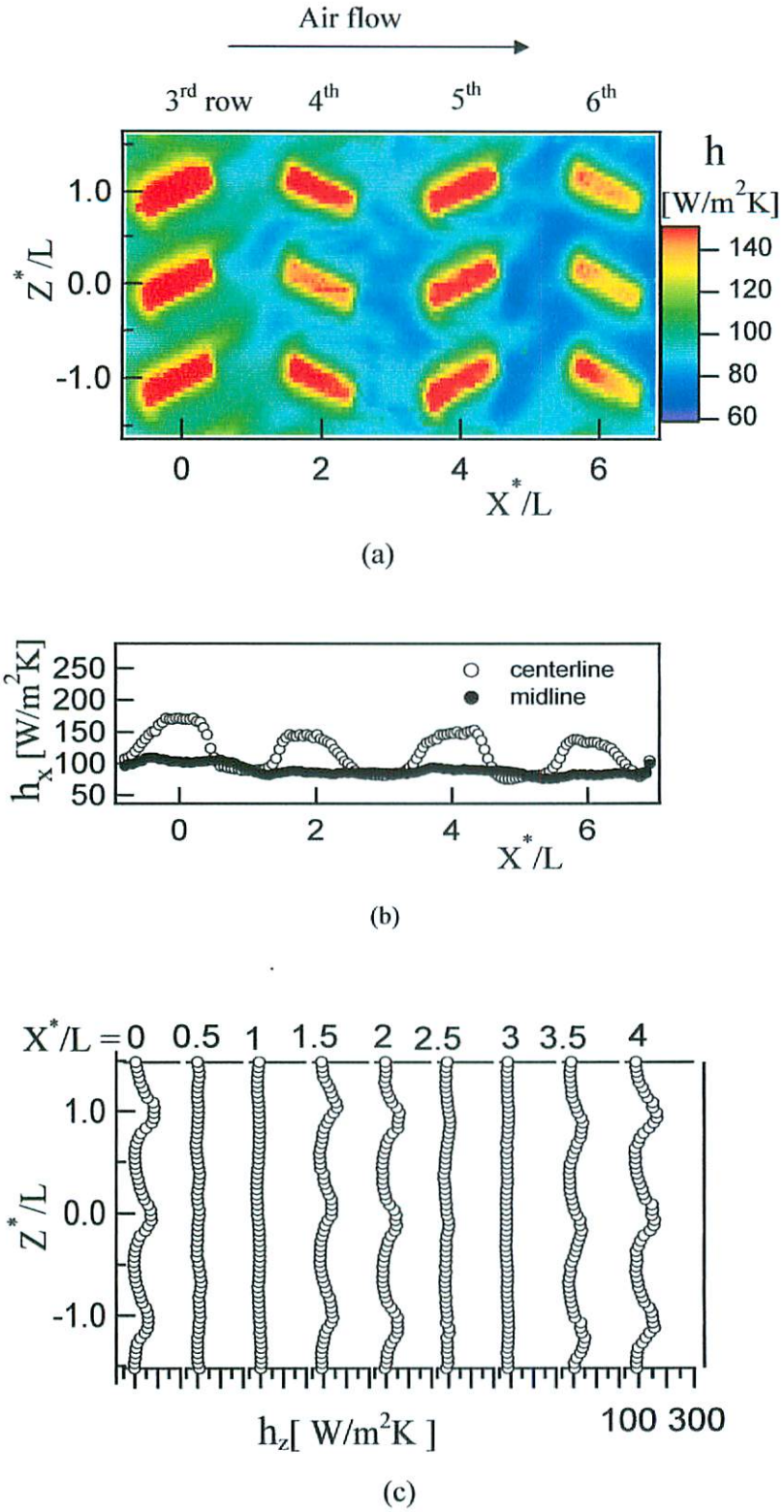


Fig.4.7 Detailed heat transfer coefficient distributions around the representative fins of zigzag pattern at the endwall in a flat plate boundary layer for $Re_L = 1.27 \times 10^4$, $H_f = 10$ mm. (a) Infrared image. (b) Centerline and midline distribution and (c) Spanwise distribution.

For both patterns, the centerline distribution is periodic and the peak indicates the $h_x$ value at the fin center. Heat transfer distributions along streamwise and spanwise with varying velocity were also found periodical regardless of fin pattern and velocity in the previous experimental work of Islam et al [2006]. Around the third row fins the distributions show higher values of $h_x$, followed by a subsequent decline in the downstream region. The slope of the decline is greater for the co-angular pattern than for the zigzag pattern. The midline distribution, showing the endwall heat transfer, is almost flat and is nearly half the maximum value. It is also notable that the slope of the decline is again higher for the co-angular pattern. The lesser slope for the zigzag pattern might be due to the vortex that strongly attaches to the farthest row fin.

Figs. 4.6(c) and 4.7(c) show the spanwise distribution for both patterns. The trends of the distributions are similar, but the values of $h_z$ are different. At $X^*/L = 0$, 2 and 4, i.e. at the center of each fin row, periodic distributions appear. At the upstream side fins the lower peak and higher peak values are higher for the co-angular pattern, but at the downstream side fins the zigzag pattern exhibit higher values. At $X^*/L = 0.5$ and 2.5, the distributions tend towards being flat while at $X^*/L = 1$ and 3, they become nearly completely flat. Immediately before the fins, i.e at $X^*/L = 1.5$ and 3.5, the distributions again become periodic. Figs. 4.8 and 4.9 show the distributions for narrow duct flow. A comparison between Figs. 4.8(a) and 4.9(a) identifies the different shapes of the heat transfer profile. In the case of the co-angular pattern, the lower heat transfer regions are comparatively large and hysterisis shaped, while for the zigzag pattern, the lower heat transfer regions are comparatively small with a delta shape. The horseshoe vortexes around the fin for both patterns observed for the oil film flow agree with the observed higher heat transfer region around the fin in the infrared images. The level of heat transfer increases in a narrow duct compared to a flat plate because the upper wall induces the flow vortex to attach to the endwall and fin surface more strongly. Large higher heat transfer regions around each fin row are observed for both patterns. Figs. 4.8(b) and 4.9(b) show the distribution along the centerline and midline. Though the patterns of the distributions are similar to those for the flat plate case, $h_x$ is greater and there is no significant decline.

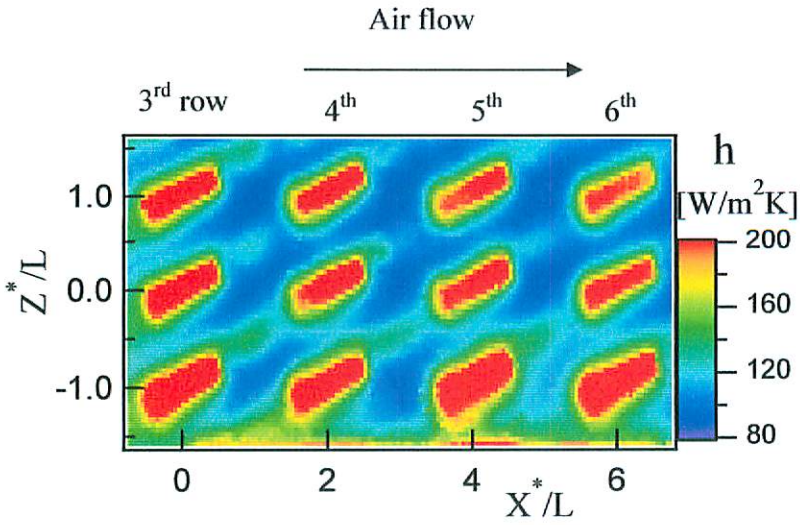


(a)

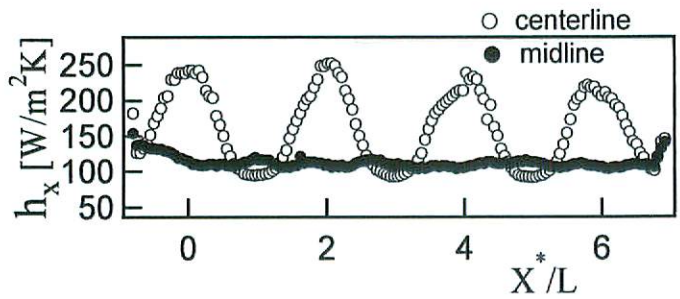


(b)

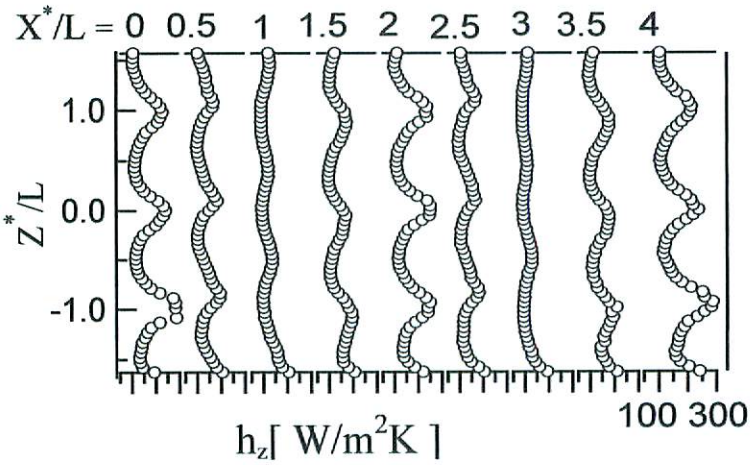


(c)

Fig. 4.8 Detailed heat transfer coefficient distributions around the representative fins of co-angular pattern at the endwall in a duct flow for $Re = 2.34 \times 10^4$, $H_f = 10$ mm. (a) Infrared image. (b) Centerline and midline distribution and (c) Spanwise distribution.

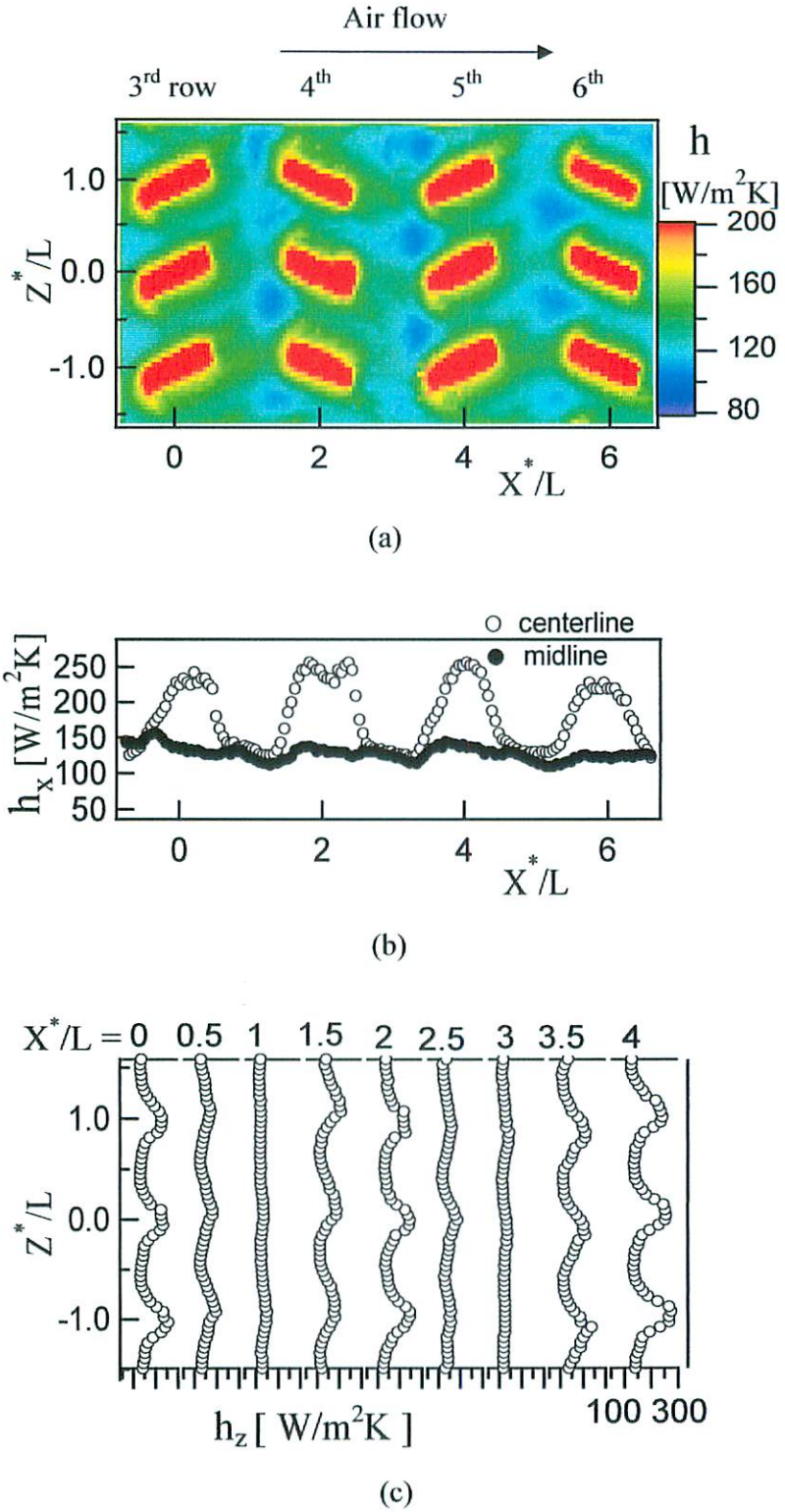


Fig. 4.9 Detailed heat transfer coefficient distributions around the representative fins of zigzag pattern at the endwall in a duct flow for $Re = 2.34 \times 10^4$, $H_f = 10$ mm. (a) Infrared image. (b) Centerline and midline distribution and (c) Spanwise distribution.

The lower peak profiles are convex for the co-angular pattern, while in contrast the profile is flat for the zigzag pattern and the lower peaks are comparatively higher. The midline distribution is nearly straight for both patterns but the $h_x$ values are greater for the zigzag pattern. Figs. 4.8(c) and 4.9(c) show the spanwise distribution for both patterns. The distribution is almost periodic except at $X^*/L$ = 1 and 3. Both the lower and higher peak profiles are comparatively more convex for the co-angular pattern, while for the zigzag pattern the profiles are higher and somewhat flat.

### 4.4. Area- averaged heat transfer

The area-averaged heat transfer coefficients at the endwall, fin base and the overall surfaces of the representative third, fourth, fifth and sixth row fins were measured from infrared images. Heat transmission from the overall surface is the total heat transfer from the fin surface and the endwall without the fins. Again heat transfer rate from the fin surface is equal to the heat transfer from fin base. So the area averaged heat transfer can be calculated using the following equation, Eq.4.3.

$$\bar{h}_{overall} = \frac{A_{fin}}{A_{overall}} \bar{h}_{fin} + \frac{A_{endwall}}{A_{overall}} \bar{h}_{endwall}, \qquad (4.3)$$

where, $A_{overall}$ is the overall surface area including the fin base and $A_{fin}$ and $A_{endwall}$ are the surface areas of the fin base and endwall, respectively. The relationship between the area-averaged Nusselt number and the Reynolds number is shown in Fig. 4.10. The area-averaged Nusselt number is represented by the curve fitted lines. All the data fall smoothly on the curve fitted lines and can be well represented by the following equation, Eq.4.4.

$$\overline{Nu} = cRe^{0.7}. \qquad (4.4)$$

Values for $c$ for different duct heights and fin patterns are listed in Table 1. It is found that the zigzag pattern has higher $c$ values. Fig. 4.10(a) shows the variation of the Nusselt number with the Reynolds number at the endwall and the overall surface for both patterns for a narrow duct,

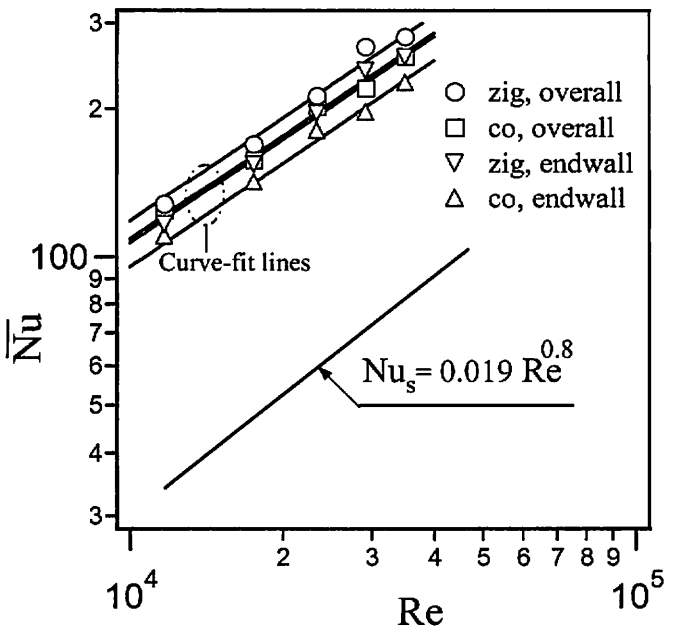


(a) Area–averaged Nusselt number at the overall surface and the endwall as a function of the duct Reynolds number for $H_d$ = 20 mm.

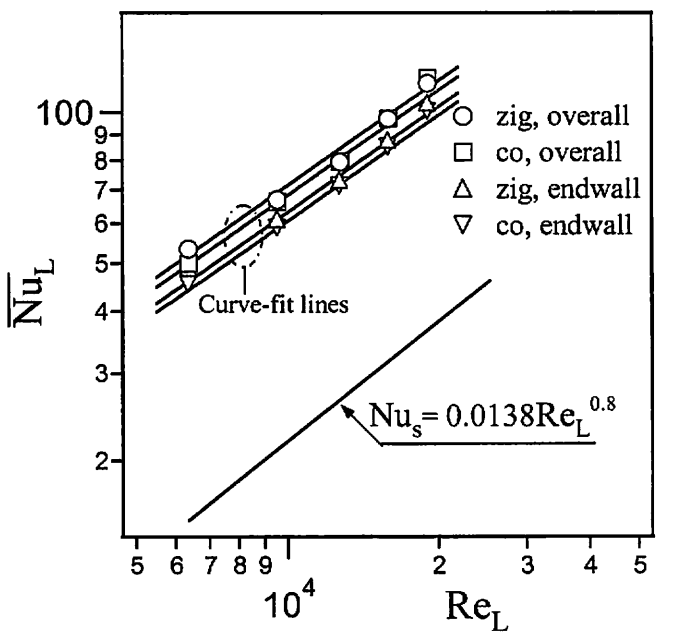


(b) Area–averaged Nusselt number at the overall surface and the endwall as a function of the Reynolds number based on fin length for $H_d$ = 200 mm.

Fig. 4.10 Relationship between Nusselt number and Reynolds number

**Table 1** Coefficient of heat transfer correlation at tall duct and narrow duct for co-angular and zigzag pattern

| Fin Pattern | Duct Height (mm ) | $\overline{Nu} = cRe^{0.7}$ | |
|---|---|---|---|
| | | $c$ | |
| | | endwall | overall |
| Co-angular | 20 | 0.151 | 0.169 |
| Zigzag | 20 | 0.17 | 0.187 |
| Co-angular | 200 | 0.096 | 0.113 |
| Zigzag | 200 | 0.100 | 0.108 |

where the Nusselt number is arranged by duct hydraulic diameter. For all cases, the Nusselt number increases with Reynolds number. Considering the overall heat transfer, the zigzag pattern shows a higher value than the co-angular pattern. As noted previously, this is due to the fact that for the zigzag setting the longitudinal vortex strikes the endwall and the fin surface more strongly up to the farthest fin row. Comparing the endwall heat transfer, the difference in the heat transfer between the co-angular and zigzag patterns is more than the difference in the overall surface area, indicating that the endwall heat transfer is more significant for the zigzag pattern while the extended surface (fin) effect is significant for the co-angular pattern. The overall heat transfer is found to be enhanced by more than four times the smooth surface value.

The variation in the Nusselt number with Reynolds number at the flat plate boundary layer is shown in Fig. 4.10(b), with the Nusselt number arranged by fin length. The overall heat transfer enhancement for both fin patterns is nearly the same though the coefficient $c$ for the zigzag pattern is somewhat higher. The endwall heat transfer for the two fin patterns is found similar too.

The heat transfer from a smooth surface was estimated as follows: The heat transfer coefficients were first calculated from the Eq. (4.1) for the flat plate boundary layer within the range $X = 0.28$ m $- 0.36$ m, corresponding to the length between the third and fifth rows.

$$\overline{h} = \int_{0.28}^{0.36} 0.0296 \mathrm{Re}_x^{0.8} \mathrm{Pr}^{0.6} \frac{\lambda}{x} .dx . \qquad (4.5)$$

These heat transfer coefficients were then replaced by the mean Nusselt number based on fin length and can be represented by the following equation:

$$\overline{Nu_L} = 0.0138 Re_L^{0.8}. \qquad (4.6)$$

The overall heat transfer was then compared and found to be more than three times the smooth surface value. Hence, it was found that heat transfer is improved with the use of fins. A zigzag pattern for $H_d$ = 20 mm was found to be most effective for heat transfer enhancement.

### 4.5 Flow visualization by dye flow in water channel

In order to differentiate the flow behavior of the co-angular and zigzag pattern, dye flow in water channel was observed at lower Reynolds number. The dye flow patterns for the co-angular and zigzag patterns are shown in Fig. 4.11. In the case of the co-angular pattern, the dye flow stagnates in front of the first row fin and forms a horseshoe vortex surrounding the fin. At the rear of the fin, the vortex rolls up and rises to join the flow separated from the upstream portion of the fin, where it then shows longitudinal behavior. As the fins are set at an angle, edge effects are observed. The corner edges cause turbulence and enhance flow mixing in the inter fin region along the streamwise direction. The main vortex flows above the fins as shown in Fig. 4.11(a), touching the top of the fins and the sidewall. The horseshoe vortex around the co-angular pattern is so strong that the longitudinal vortex cannot contact the inner portion of the horseshoe vortex and the vicinity of the endwall except for the both side walls of the fins. It causes heat transfer enhancement from the surface.

In the case of the zigzag pattern shown in Fig. 4.11(b), a longitudinal vortex generated by the first fin row touches the front of the second row fin and attaches to the endwall around the fin as the horseshoe vortex that appears is not strong. Due to the alternate directions of the fins, the flow direction is changed and the longitudinal vortex strikes the endwall between the second and

third row fins. The inter fin region in the spanwise direction at the third row is contacted by the main vortex. Beyond this row, the flow advances and touches the following fin and the endwall. We note that the flow attaches strongly to both sides of the fin for the co-angular pattern, while for the zigzag pattern the front side is touched by the flow strongly but the back side is softly touched only. Therefore, heat transfer from the fin should be significant in the co-angular case, while heat transfer from the endwall should be higher in the case of the zigzag pattern,as will be described later

.

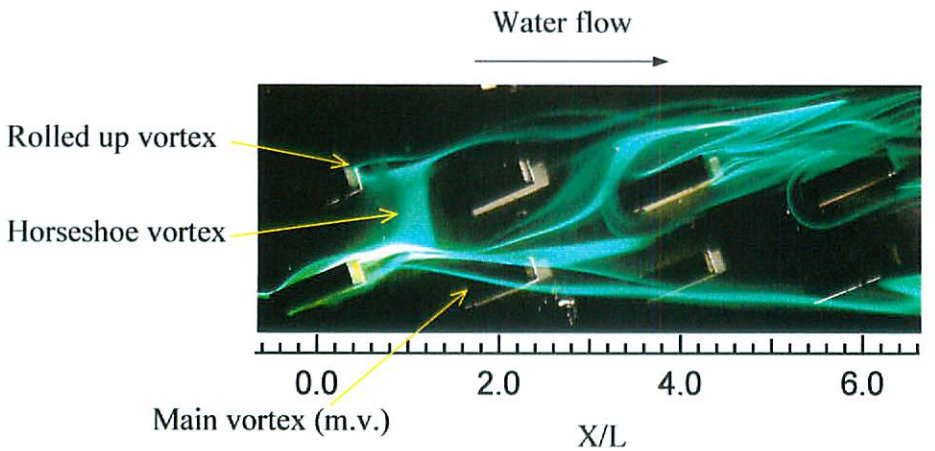


(a)

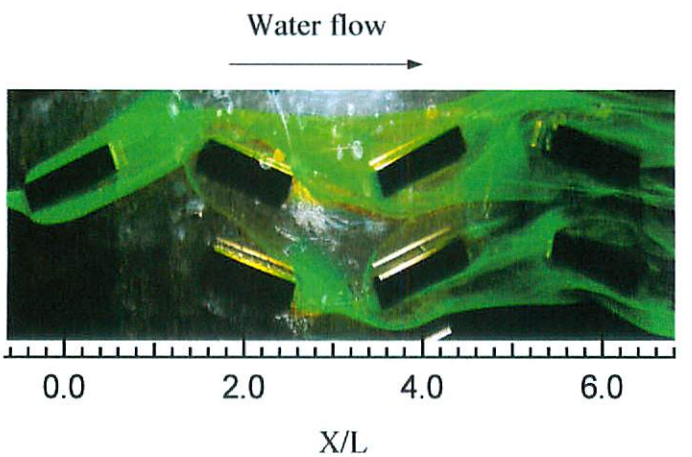


(b)

Fig. 4.11 Flow visualization in a water channel around short rectangular fin of (a) co-angular, (b) zigzag pattern with $H_f$ = 10 mm, $PR$ = 2 and $Re$ = 1350.

### 4.6. Friction factor

In order to calculate friction factor, we first measured the pressure drop distribution. Fig.4.12 shows the friction factor obtained from Eq. (3.1) in a narrow duct. In the tall duct, a hydrodynamic boundary layer does not fully develop. The friction factor for large scale protrusion positioned in surface shows almost constant regardless of the Reynolds number and the friction factor values for both patterns are larger due to the large scale vortex formed by the existing protrusions than the skin friction for a smooth duct without fins for fully developed turbulent flow. As the flow for the zigzag pattern has more contact with the fin surface and endwall and consequently a larger drag force occurs than for the co-angular pattern. As a result the friction factor, $f$ is somewhat higher for the zigzag pattern than that of co-angular pattern.

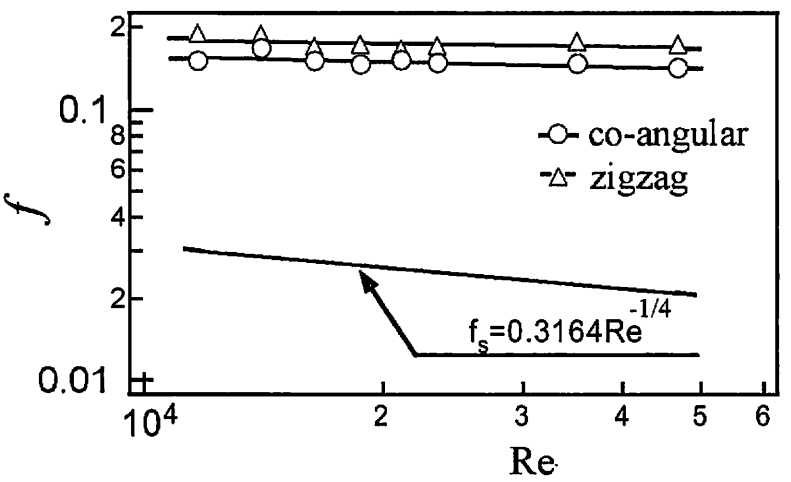


Fig. 4.12 Friction factor vs. Reynolds number in a narrow duct for co-angular and zigzag pattern of $H_f$ = 10 mm

### 4.7 Summary

After performing this investigation we can conclude as follows:

1. The inclination angle has a great influence on the heat transfer enhancement. Among the inclination angles of 0°, 20° and 25°, an angle of 20° appears optimum for enhancement in this experiment.
2. The friction factors for both patterns were larger compared with the skin friction on the smooth surface for a fully developed turbulent flow. The friction factor value was found to be almost constant and larger for a zigzag pattern of fins than for a co-angular pattern.
3. In dye flow, strong longitudinal vortexes appeared that touch the endwall near the inter fin space. In the case of the zigzag pattern, one side of the fin was also contacted by the vortex. Though a corner vortex also touches the side wall of the fin, the horseshoe vortex was not as clearly observed. In contrast, a longitudinal vortex is also observed for the co-angular pattern, which touches the fin surface as well as lightly contacting the endwall. A horseshoe vortex is also clearly observed in front of the fins.
4. Comparing arrays of co-angular and zigzag patterns, the later is more effective for heat transfer enhancement in the case of narrow duct flow. The average heat transfer coefficient for a zigzag pattern is more than four times higher than that of without fins. The Nusselt number increases with Reynolds number to the $0.7^{th}$ power for both patterns in a narrow duct as well as for a flat plate boundary layer.